verse problem (*7, 10, 13, 14*). Slip rates at depths of the repeating sequences cannot be resolved by other methods, so recurrence-determined rates in joint inversion with surface deformation can provide constraints for fault slip throughout the full depth range of the fault. With microearthquake observations made at distances of 10 to 20 km slip-rate, changes of a few millimeters per year can be resolved. We view each sequence as a point detector of local slip on the fault.

Our analysis suggests that a propagating concentration of accelerated slip entered the Parkfield segment of the San Andreas fault from the northwest in 1988 and moved along the fault zone to the southeast, leaving the area in 1998. It moved through the hypocentral region of the most recent magnitude 6 Parkfield earthquakes, triggering a succession of increasingly energetic episodes of slip-induced seismicity, and culminated with near complete relaxation in that region. The only part of the fault showing slip rates in 1998 greater than pre-1989 levels was the southeasternmost section at 8 to 10 km depth, as if the slip pulse had moved beneath the locked section of the fault. Throughout all this change, the repeating microearthquake waveforms did not vary measurably, precluding substantial change in earthquake source parameters or medium properties at the sources. Local conditions, other than loading rates, remained essentially constant at the asperities, and processes that would result in fluctuations in source size, such as fault strengthening with contact time (fault healing), although detectable, were very small (*15*).

The utility of the recurrence-derived slip-rate distribution lies in its monitoring potential for processes at depth in active fault zones. It remains to be determined whether the correlation of slip-rate variations and microearthquake occurrence found at Parkfield exists elsewhere, if the method can be extended in time (to decades and centuries) and space (hundreds of kilometers) for application to large damaging earthquakes, and whether the precursory changes in the relative abundance of repeating sequences of microearthquakes is a basic phenomenon in the earthquake cycle. There are few high-resolution networks in place today to test this at magnitudes approaching zero, where recurrence times are less than a few years and thus readily detected.

References and Notes

1. W. H. Bakun and A. G. Lindh, *Science* **229**, 619 (1985).
2. R. M. Nadeau, W. Foxall, T. V. McEvilly, *ibid.* **267**, 503 (1995); R. M. Nadeau and T. V. McEvilly, *Bull. Seismol. Soc. Am.* **87**, 1463 (1997).
3. R. M. Nadeau and L. R. Johnson, *Bull. Seismol. Soc. Am.* **88**, 790 (1998).
4. W. L. Ellsworth, in *Urban Disaster Mitigation: The Role of Science and Technology*, F. Y. Cheng and M. S. Sheu, Eds. (Elsevier, Oxford, 1995); D. P. Schaff, G. C. Beroza, B. E. Shaw, *Geophys. Res. Lett.* **25**, 4549 (1998). In sequences of similar aftershocks, seismic moment release and recurrence rates were related to measured surface deformation and loading rate at depth to investigate post-seismic deformation. An aftershock sequence differs from the more nearly steady-state microearthquake occurrence seen at Parkfield.
5. J. B. Fletcher and P. Spudich, *J. Geophys. Res.* **103**, 835 (1998).
6. E. Karageorgi, T. V. McEvilly, R. Clymer, *Bull. Seismol. Soc. Am.* **87**, 39 (1997); E. G. Quilty and E. A. Roeloffs, *ibid.*, p. 310.
7. J. Langbein, R. Gwyther, R. Hart, M. T. Gladwin, *Geophys. Res. Lett.*, in press.
8. The triggered network can fail to capture an event for a number of reasons, introducing artificially lengthened T_{av} and (typically doubled) T values. The bimodal nature of T_{av}, for subsets before and after 1992, broadens the peak. The combined effects are evident in Fig. 2.
9. M varies little throughout a sequence compared with T, and results based on individual M values at either the beginning or at the end of the T_i intervals are indistinguishable from those based on M_{av}.
10. R. A. Harris and P. Segall, *J. Geophys. Res.* **92**, 7945 (1987).
11. J. Langbein, unpublished data. Short baseline creepmeters do not measure the off-fault deformation present in the creep-to-locked transition zone.
12. As the sampling window approaches the end of the database, progressively more open-ended intervals are encountered and T_i is unknown because the next event in the sequence has not yet occurred.
13. J. O. Langbein, R. O. Burford, L. E. Slater, *J. Geophys. Res.* **95**, 2533 (1990).
14. R. E. Burgmann, R. E. Fielding, J. Sukhatme, *Geology* **26**, 559 (1998).
15. We found an 18% increase in M for a 10-fold increase in the preceding T_i, supporting a fault-healing process. Laboratory data suggest 3 to 8% for a 10-fold increase in recurrence interval [J. Dieterich, *J. Geophys. Res.* **77**, 3690 (1972); C. Scholz, P. Molnar, T. Johnson, *ibid.*, p. 6382; C. Scholz and T. Engelder, *Int. J. Rock Mech. Miner. Sci.* **13**, 149 (1976)].
16. Supported by the U.S. Geological Survey through award 1434-95-G2540. Data processing at the Lawrence Berkeley National Laboratory was supported by the U.S. Department of Energy Office of Basic Energy Sciences. Partial support (R.N.) came from the Lawrence Livermore National Laboratory Institute of Geophysics and Planetary Physics Campus–Laboratory Collaboration project.

19 February 1999; accepted 11 June 1999

Detection of Low-Temperature Hydrothermal Fluxes by Seawater Mg and Ca Anomalies

Stephanie de Villiers* and Bruce K. Nelson

Geochemical fluxes into and out of the ocean control its chemical composition. Measurements of the magnesium (Mg) content of seawater, an assumed "conservative" element in the ocean, reveal mid-depth Mg depletions in the vicinity of the East Pacific Rise. The magnitude of the anomalies suggests that fluxes associated with the low-temperature circulation of seawater through axial mid-ocean ridge systems are much larger than the high-temperature axial component. A higher total axial hydrothermal flux provides a mechanism that simultaneously satisfies the mass balance requirement of several major seawater constituents.

The most abundant elements enter the oceans dissolved in river water and in high-temperature (HT) hydrothermal flows at mid-ocean ridge spreading centers and are removed by calcium carbonate deposition, loss at the air-sea interface, and evaporite deposition. Given the best estimates of the global magnitude of these fluxes (*1–3*), inputs exceed outputs by perhaps a factor of 4 in the case of sodium, a factor of 2 to 10 in the case of magnesium and sulfate, and a factor of 20 for potassium. In contrast, calcium is apparently removed from the ocean at twice the rate it is supplied (*4*). Either the ocean is far removed from a steady state with respect to all major elements—accumulating Na^+, Mg^{2+}, K^+, and SO_4^{2-}, while decreasing in Ca^{2+}—or one or more significant geochemical fluxes are unrecognized or poorly constrained. Here we present evidence for the existence of the proposed large low-temperature (LT) component of hydrothermal circulation at a mid-ocean ridge axial system (*5, 6*).

Recent water column profiles show an excess of Ca over that predicted by alkalinity (*7*). It has been hypothesized that the inferred excess Ca flux originates in LT, diffuse, on-axis flows, exceeding the better documented HT discrete axial flux by a factor of up to 10 (and comparable to river input). The LT flux simultaneously resolved the Ca alkalinity discrepancy and balanced the oceanic Ca cycle (*4*). LT flux should also be an important component of other major element cycles.

It has been inferred that LT hydrothermal processes act as a sink of unknown magnitude for the other major seawater elements: Na^+, Mg^{2+}, K^+, and SO_4^{2-} (*6, 8*), a hypothesis that is qualitatively consistent with observed deficiencies that have been noted in mass balance models of a steady-state ocean (*1–3*). Thus, the

---

Geological Sciences Department, Box 35-1310, University of Washington, Seattle, WA 98195-1310, USA.

*Present address: Department of Geological Sciences, University of Cape Town, Rondebosch 7701, South Africa. E-mail: steph@cigc.uct.ac.za

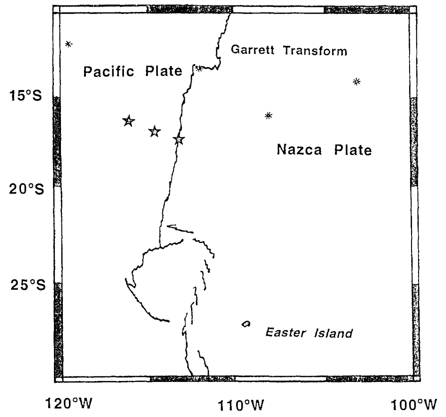

Fig. 1. Water samples were collected in the eastern South Pacific Ocean at the three stations indicated with a star: A, at 16°23'S, 115°59'W (depth 3188 m); C, at 16°42.50'S, 114°37'W (depth 3089 m); and J, at 17°00.30'S, 113°05.70'W (depth 2648 m). For comparison, the He profiles of (*11*) were collected at the stations indicated with an asterisk.

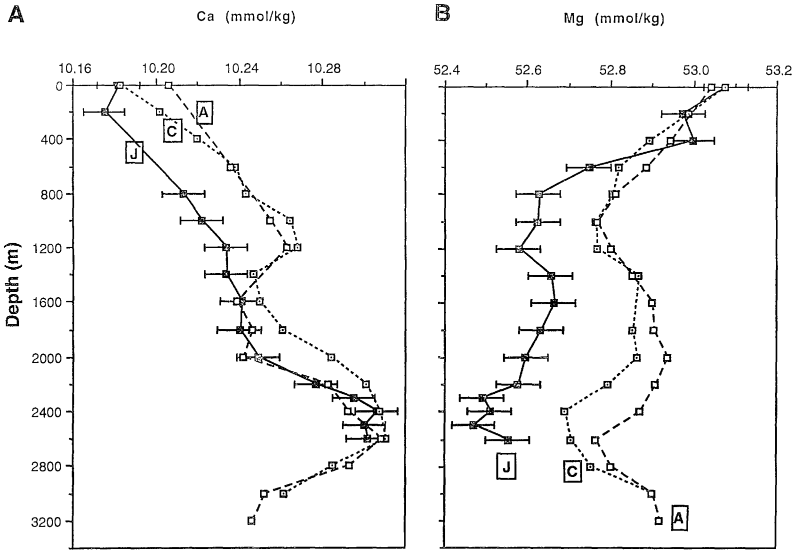

Fig. 2. (**A**) Calcium concentration profiles at the three sample stations shown in Fig. 1, normalized to a salinity of 35 and obtained by the isotope-dilution thermal ionization mass spectrometry (TIMS) method described in (*7*). The error bars on profile J represent a 1σ measurement precision of 0.09%. (**B**) Magnesium concentration profiles at the three sample stations shown in Fig. 1, normalized to a salinity of 35 and obtained by the isotope-dilution TIMS method described (*9*). The error bars on profile J represent a 2σ measurement precision of 0.1%.

LT hypothesis also predicts inversely correlated seawater concentrations of Ca with respect to elements such as Mg; however, existing data indicate that Mg behaves conservatively in seawater. To test this prediction, we collected seawater depth profiles for Ca and Mg analyses, and we developed a high-precision mass spectrometric analytical technique for Mg and Ca (*9*). We sampled the water column above the southern East Pacific Rise (EPR) (Fig. 1) where, on the basis of spreading rate, we expected the anomalies predicted by the hydrothermal hypothesis to be the most pronounced.

We sampled three water column profiles along a transit 300 km long, extending west from the East Pacific Rise at 17.5°S (Fig. 1). At a depth of 2200 to 2600 m, which is the depth of the ridge crest, dissolved Ca concentrations (normalized to salinity) are elevated up to 50 μM above that at the upper boundary of the linear potential temperature–salinity (T_p-S) region (1600 m in Fig. 2A). These enhanced Ca concentrations cannot be attributed to calcium carbonate dissolution, as that would require an analogous mid-depth maximum in alkalinity on the order of 100 microequivalents per kilogram (μeq/kg), which is far higher than any observed (~25 μeq/kg) in this region (*10*). A secondary pool of water also enriched in Ca is observed at a depth of 1000 to 1200 m above the ridge crest (Fig. 2A). This feature is situated below the Antarctic Intermediate Water mass, as defined by its low-salinity characteristics.

Magnesium analyses (*9*) show an inverse relation between Mg and Ca (Fig. 2B). The strongest vertical gradient in Mg (normalized to salinity) is in the profile closest to the ridge axis. Water sampled about 50 m above the crest is depleted by up to 0.55 mM, or 1%, relative to surface values of 53 mM. At stations farther west or downcurrent from the ridge, the water column is on average less depleted in Mg, although the mid-depth plume remains well defined over the length of the transect. The Mg/Ca ratio of seawater decreases by more than 2% (Figs. 3 and 4); that is, Ca and Mg concentration vary inversely. This evidence implies that the concentration of Mg, the second most abundant cation in seawater, varies. The strong inverse correlation of Mg with Ca is consistent with one of the predictions of the hydrothermal hypothesis and is strong evidence that the source of this variability is the hydrothermal fluid flux.

As Mg concentrations away from the ridge axis increase toward high background values, Ca concentrations remain approximately constant or slightly increase instead of showing an expected decrease toward its low background values (Figs. 2 and 3); that is, the data do not form a simple two-endmember mixing line. The likely reason is that for elements or isotopes such as Mg and ^{3}He, in situ addition or loss of nonhydrothermal origin is negligible in the deep ocean (that is, additions of Mg from calcium carbonate dissolution and eventual loss of ^{3}He to the atmosphere). Therefore, away from the ridge crest, the spatial distribution of the hydrothermal signal for these elements depends primarily on the extent to which it is mixed out against seawater with higher Mg and lower ^{3}He values.

However, Ca and other seawater components have both a hydrothermal source (or sink) and an in situ flux (for example, biogenic calcium carbonate or silicate dissolution), and these will continue to undergo addition (or depletion in the case of particle-reactive components) away from the ridge crest. This causes apparent decoupling of the hydrothermal signal for Ca versus Mg and for Ca versus ^{3}He (Figs. 2 and 3) (*11*) away from the ridge crest. The manner in which the temperature anomaly associated with the hydrothermal heat flux propagates is even more complex. For seawater properties as fundamentally different as temperature, He, Ca, and Mg, this effect must be considered when investigating large-scale distribution patterns and water column profiles for evidence of hydrothermal input.

The axial hydrothermal flux is composed of a HT (discrete) component and a LT (diffuse) component. The integrated heat flux associated with the LT diffuse axial flows is estimated to exceed the HT discrete axial component by an order of magnitude (*5*). Similarly, the water flux associated with LT diffuse flow may exceed the HT water flux by perhaps as much as three orders of magnitude (*6*, *8*). Little is known about the chemistry of LT diffuse fluids; however, available data suggest that LT fluids contain chemical anomalies of sufficient magnitude to generate large chemical fluxes (*6*, *12*, *13*). Of particular importance are suggestions that LT circulation does not have significant ^{3}He concentrations (*8*, *11*) and that ratios of other elements to ^{3}He (for example, Si and CO$_2$) in LT fluids exceed those in HT fluids by about an order of magnitude (*13*). These data imply that the measured mid-depth Ca enrichments and Mg depletion represent the combined effect of LT and HT hydrothermal fluxes and that we may calculate their relative contributions by using ^{3}He as a tracer of the HT component.

If we assume that ^{3}He is present predominantly in the HT flux (*11*), documented δ^3He profiles can be used to predict the associated Ca

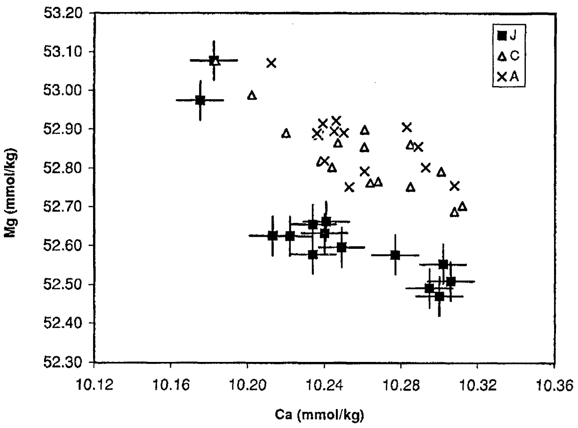

Fig. 3. Scatter plot of Mg versus Ca for the three profiles shown in Fig. 2. The error bars indicate a 1σ measurement precision. From this it can be seen that all the Ca and Mg data do not fall on a simple two-endmember mixing line, which is the result of Ca undergoing addition from calcium carbonate dissolution, as discussed in the text.

and Mg water column anomalies. The closest documented transect is several hundred kilometers away (*11*), and greater concentrations are expected closer to 17.5°S. Dilutions and anomalies calculated based on a 20 to 60% mid-depth δ^3He maximum (*11*) should therefore be considered lower estimates of the HT component. Given a range in HT fluid endmember concentrations of 2×10^{-6} to 23×10^{-6} μM (*14*, *15*), the mid-depth ^{3}He anomalies (*11*) indicate a range of seawater/HT fluid mixing ratios of ~1300:1 to 19,000:1. For HT fluid Ca concentrations of 20 to 40 mM (*15*, *16*), these seawater/HT fluid ratios predict that a Ca concentration anomaly of 2 to 23 μM should accompany the ^{3}He anomaly. This is only 10 to 50% of the signal observed above the EPR (Fig. 2A). Similarly, if we assume that Mg is completely removed from hydrothermal fluids, the inferred seawater/HT fluid ratios predict an associated mid-depth Mg depletion anomaly of 3 to 40 μM. This range is at least an order of magnitude less than the measured 500 μM depletion (Fig. 2B). Both the Ca and Mg mid-depth anomalies imply that the total hydrothermal flux greatly exceeds the flux predicted from ^{3}He data and that the LT Mg flux may exceed the HT Mg flux by perhaps as much as a factor of 10. Early ^{3}He-based estimates of the hydrothermal Mg flux (*15*, *17*) suggested values of 7.5×10^{12} to 9.3×10^{12} mol/year, which is consistent with mass balance estimates of 6×10^{12} to 8.5×10^{12} mol/year if the ocean is assumed to be at a steady state (*18*). More recent estimates based on revised ^{3}He/heat ratios suggest much lower values of 0.5×10^{12} to 2×10^{12} mol/year (*6*, *8*, *19*). Despite the large uncertainties in these estimates, the mid-depth Mg anomalies are therefore consistent with mass balance requirements if the ocean is at a steady state. The Mg anomaly–based estimate of the LT:HT flux ratio, combined with recent estimates of the global HT ^{3}He flux (*19*) compared to the requirements of the oceanic Mg mass balance, is also consistent with that predicted by axial heat flow measurements and by estimates of LT versus HT water fluxes (*5*).

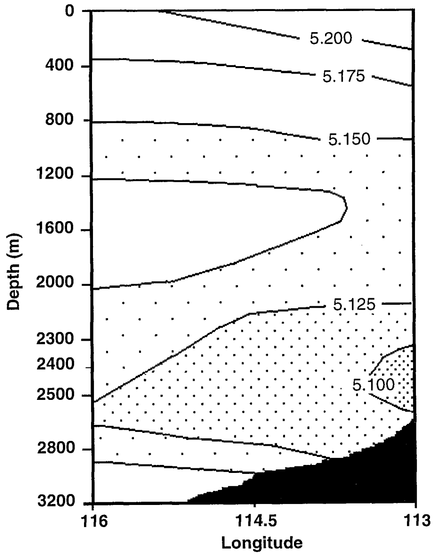

Fig. 4. Contour diagram of seawater Mg/Ca ratios (mole/mole) along the transect shown in Fig. 1. Contour intervals are in increments of 0.025 mol/mol. The black area in the lower right corner represents the ridge crest.

The translation of Mg and Ca anomalies over specific depth intervals into an implied hydrothermal flux contains an important caveat: it assumes that the HT and LT components of the mid-depth plume are established over a similar time interval. In the case of ^{3}He, its escape rate from the atmosphere provides some measure of the degassing flux required to maintain He in the atmosphere, assuming a steady state. In the case of LT axial fluxes, we do not have a measure of the time over which the water column Mg and Ca anomalies were established, other than that inferred from measured and estimated LT/HT heat flux measurements. The more diffuse nature of LT flows complicates establishing how it is incorporated into the steady-state plume. Furthermore, we do not know how important recirculation is to establishing water column anomalies, nor the extent to which the "background" against which anomalies are calculated already represents a LT flux component. The answers to these questions are essential to establishing the importance of the total hydrothermal flux to the composition of seawater.

References and Notes

1. H. D. Holland, *The Chemical Evolution of the Atmosphere and Ocean* (Princeton Univ. Press, Princeton, NJ, 1984).
2. J. I. Drever, Ed., *Sea Water: Cycles of the Major Elements* (Dowden, Hutchinson & Ross, Stroudsburg, PA, 1977); E. K. Berner and R. A. Berner, *The Global Water Cycle: Geochemistry and Environment* (Prentice-Hall, Englewood Cliffs, NJ, 1987); M. E. Q. Pilson, *An Introduction to the Chemistry of the Sea* (Prentice-Hall, Upper Saddle River, NJ, 1998).
3. L. A. Hardie, *Geology* **24**, 279 (1996); H. D. Holland, H. Horita, W. E. Seyfried, *ibid.*, p. 993.
4. J. D. Milliman, *Global Biogeochem. Cycles* **7**, 927 (1993).
5. A. Schultz, J. R. Delaney, R. McDuff, *J. Geophys. Res.* **97**, 12299 (1992); P. A. Rona and D. A. Trivett, *Earth Planet. Sci. Lett.* **109**, 57 (1992); E. T. Baker, G. J. Massoth, S. L. Walker, R. W. Embley, *ibid.* **118**, 235 (1993); A. Schultz and H. Elderfield, *Philos. Trans. R. Soc. London Ser. A* **355**, 387 (1997).
6. M. J. Mottl and C. G. Wheat, *Geochim. Cosmochim. Acta* **58**, 2225 (1994).
7. S. de Villiers, *Earth Planet. Sci. Lett.* **164**, 627 (1998).
8. H. Elderfield and A. Schultz, *Anun. Rev. Earth Planet. Sci.* **24**, 191 (1996).
9. Samples were collected at three stations (A, C, and J) west of the EPR: A, at 16°23'S, 115°59'W (depth 3188 m); C, at 16°42.50'S, 114°37'W (depth 3089 m); and J, at 17°00.30'S, 113°05.70'W (depth 2648 m). Calcium analyses were performed as described in (*6*). For Mg analyses, about 0.5 g of seawater was weighed out and equilibrated with an appropriate amount of ^{26}Mg spike solution, and the Mg fraction was separated from other sea salts by means of cation-exchange resis (Biorad AG-50, ×8). The Mg fraction was eluted, dried, and redissolved in hydrochloric acid before being loaded onto Re filaments with Ta activator. Mass fractionation was corrected for by an exponential law, and data was collected in single collector mode (VG Sector). Repeat analysis of an internal standard yielded an external measurement precision of 0.044% (1σ, $n = 10$).
10. H. G. Ostlund, H. Craig, W. S. Broecker, D. Spencer, Eds., *GEOSECS Atlantic, Pacific and Indian Ocean Expeditions* (National Science Foundation, Washington, DC, 1987).
11. J. E. Lupton and H. Craig, *Science* **214**, 13 (1981).
12. C. G. Wheat and M. J. Mottl, *J. Geophys. Res.* **99**, 3067 (1994).
13. J.-I. Ishibashi *et al.*, *Earth Planet. Sci. Lett.* **128**, 183 (1994).
14. J. L. Charlou, J. P. Donval, P. Jean-Baptiste, A. Dapoigny, P. A. Rona, *Geophys. Res. Lett.* **23**, 3491 (1996); L. Merlivat, F. Pineau, M. Javoy, *Earth Planet. Sci. Lett.* **84**, 100 (1987).
15. K. L. von Damme *et al.*, *Geochim. Cosmochim. Acta* **49**, 2197 (1985).
16. H. N. Edmonds *et al.*, *Geophys. Res. Lett.* **23**, 3487 (1996).
17. J. B. Corliss *et al.*, *Science* **203**, 1073 (1979); J. M. Edmond *et al.*, *Earth Planet. Sci. Lett.* **46**, 1 (1979).
18. M. J. de Wit and R. A. Hart, *Lithos* **30**, 309 (1993); R. M. McDuff and F. M. M. Morel, *Environ. Sci. Technol.* **14**, 1182 (1980).
19. T. J. Wolery and N. H. Sleep, in *Chemical Cycles in the Evolution of the Earth*, C. B. Gregor, R. M. Garrels, F. T. Mackenzie, J. B. Maynard, Eds. (Wiley, New York, 1988), pp. 77–103; D. Kadko, J. Baross, J. Alt, in *Seafloor Hydrothermal Systems*, S. E. Humphris, R. A. Zierenberg, L. S. Mullineaux, R. E. Thompson, Eds. (American Geophysical Union, Washington, DC, 1995), pp. 446–466.
20. Sample collection was made possible by a ship kindly provided by A. Chivas. This research was supported by NSF grant OCE-9529749.

10 March 1999; accepted 15 June 1999